Project LAUE –

Una lente per i raggi Gamma

Scientific requirements and detectors specification analysis for the Project: Laue - Una lente per i raggi Gamma

Natalia Auricchio, Ezio Caroli, John B. Stephen, Angelo Basili

Internal Report INAF/IASF-Bo n. 607/2012

TABLE OF CONTENTS

1. Subject

1.1 Purpose

The document reports the scientific requirements and detectors' specification analysis as required by Task 1 of the W.P. EGSE, integration and test.

2. Applicable and reference documents

1. [DA-01] Contratto ASI I/068/09/0 ed Allegato tecnico gestionale
2. [DA-02] Proposta Tecnico-Gestionale sottomessa ad ASI
3. [DA-03] Science Requirement (WP 1200, UNIFE-LAUE-RP-01-10)
4. [DA-04] Specifiche dell'EGSE: Definizione/Accettazione e realizzazione Rivelatore (WP 4300, IASFBO-LAUE-RP-01-10)
5. [DA-05] LAUE EGSE SOFTWARE FUNCTIONAL REQUIREMENTS FOR DETECTOR DATA PROCESSING (TAS-I)
6. [DA-06] WPD, PROJECT: LAUE – UNA LENTE PER RAGGI GAMMA, W.P. TITLE: EGSE, integration and test (TAS-I).

3. Acronyms

ASI	Agenzia Spaziale Italiana
HW	Hardware
IASFBO	Istituto di Astrofisica Spaziale e Fisica Cosmica di INAF Bologna
INAF	Istituto Nazionale di Astrofisica
LARIX	Large Italian X-ray facility
SW	Software
TAS-I	Thales Alenia Space -Italia
UNIFE	Università di Ferrara – Dipartimento di Fisica
WP/WPD	Work Package/Work Package Description

4. Introduction

The detection system to be used for positioning and gluing each crystal onto the lens petal frame and for qualification of the assembled petal is composed of two detectors: an imager and a spectrometer.

5. Imager Requirements

The imager function is to acquire the images needed to determine the Bragg angle and, therefore the average direction of the chosen lattice planes of each crystal tile. The imager requirements are reported in table 5.1 [DA-03, DA-04]:

Table 5.1. Imager requirements

Energy range (keV)	80-300
Spatial resolution (micron)	< 300
Active area (cm^2)	20x20
Detection efficiency	10% at 300 keV
Sensitivity	high due to the very low flux of the beam

The market research has allowed us to identify the following detectors:

i. X ray Image intensifiers
ii. ALS detectors
iii. Digital X-ray Flat Panel Detectors

5.1 X ray Image Intensifier detection principle

The X-ray image intensifier converts the transmitted x rays into a visible light image. Within an image intensifier, the input phosphor converts the x-ray photons to light photons, which are then converted to photoelectrons within the photocathode. The electrons are accelerated and focused by a series of electrodes so that they strike the output phosphor on the opposite side from the input screen. The output phosphor converts the accelerated electrons into light photons that may be captured by various imaging devices, for example a CCD (see Fig. 5.1, left). Through this process, several thousand light photons are produced for each x-ray photon reaching the input phosphor. Most modern image intensifiers use caesium iodide for the input phosphor as it has a high absorption efficiency. Due to design restrictions, image intensifiers are subject to inherent and induced artifacts that contribute to image degradation; in fact a drawback of this detection system is pincushion distortion, shown in Fig. 5.1 (right), due to the curved surface of the input screen. Both spatial and contrast resolution gradually decrease during the lifetime of the image intensifier because the brightness gain of an image intensifier decreases with time as the phosphor ages.

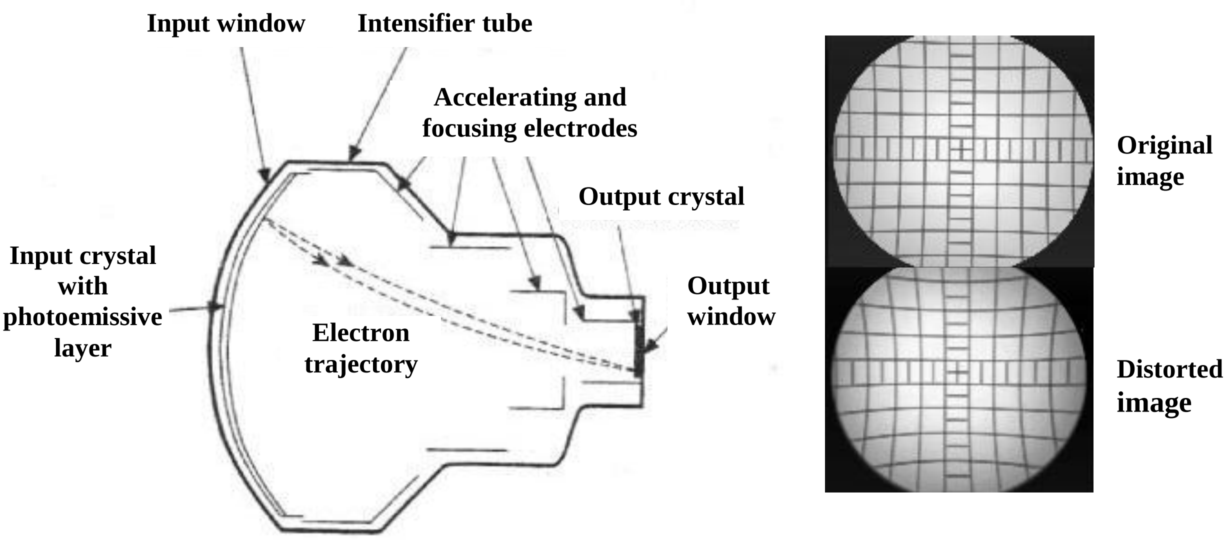

Figure 5.1. Schematic view of an image intensifier (left); pincushion distortion: comparison between the original and distorted image, caused by the curvature of the input screen of the tube (right).

We have carried out at the Larix facility two kinds of test using a radiological imaging unit TH 59432HD by THALES (see Fig. 5.2), that includes a high performance 12” image intensifier, a specifically designed high-resolution CCD camera, a dedicated single-port compact optical system and a microprocessor controlled power supply:

a) a set of measurements to evaluate the signal to noise ratio;
b) acquisition of images at high energy.

The instrument spatial resolution is 0.304 ± 0.023 mm.

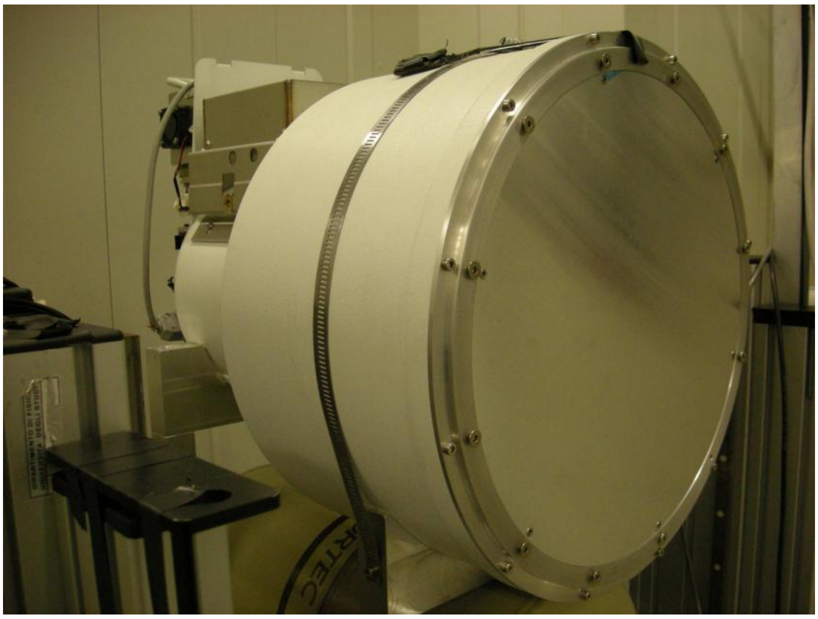
Figure 5.2. Photo of the imaging unit TH 59432HD.

a) Signal to noise ratio evaluation

We have acquired 500 images, irradiating a Cu crystal of size 15 mm x 15 mm x 2 mm in the Laue configuration with an X-ray beam at 100 keV, that simulates the betatron flux at 20 m. The integration time is 2 s for each image. We have recorded an image of the background, the transmitted beam, reported in Fig. 5.3, and the images of the diffracted beams, summed in groups of a hundred.

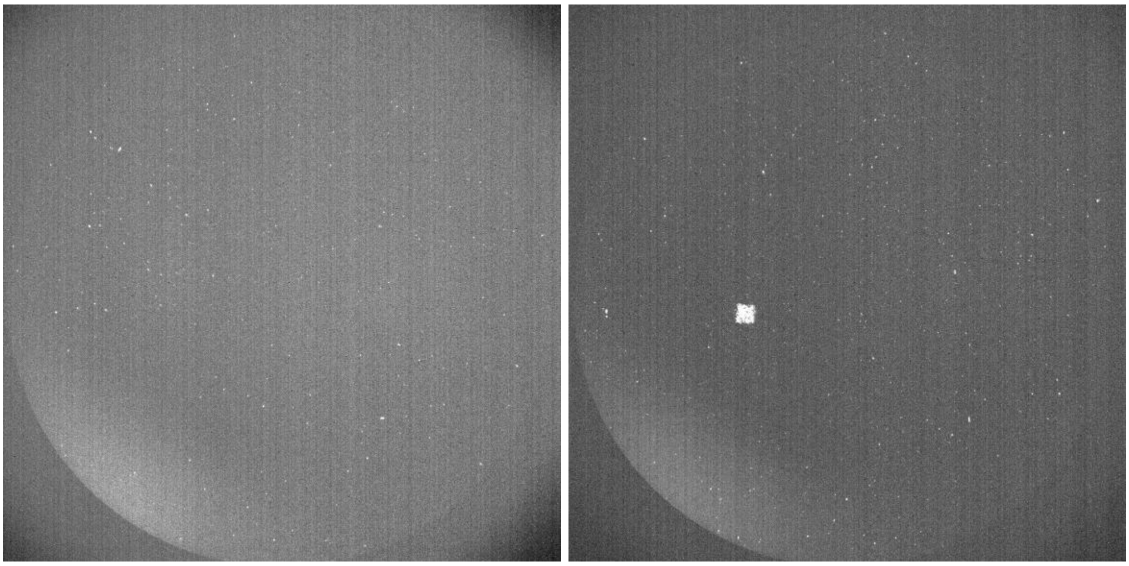
Figure 5.3. Image intensifier background (left) and transmitted beam by a Cu crystal in Laue configuration (right).

The summed images were normalized and are shown below in Figs. 5.4 and 5.5 together with the profiles obtained on the horizontal (X) and vertical (Y) axes.

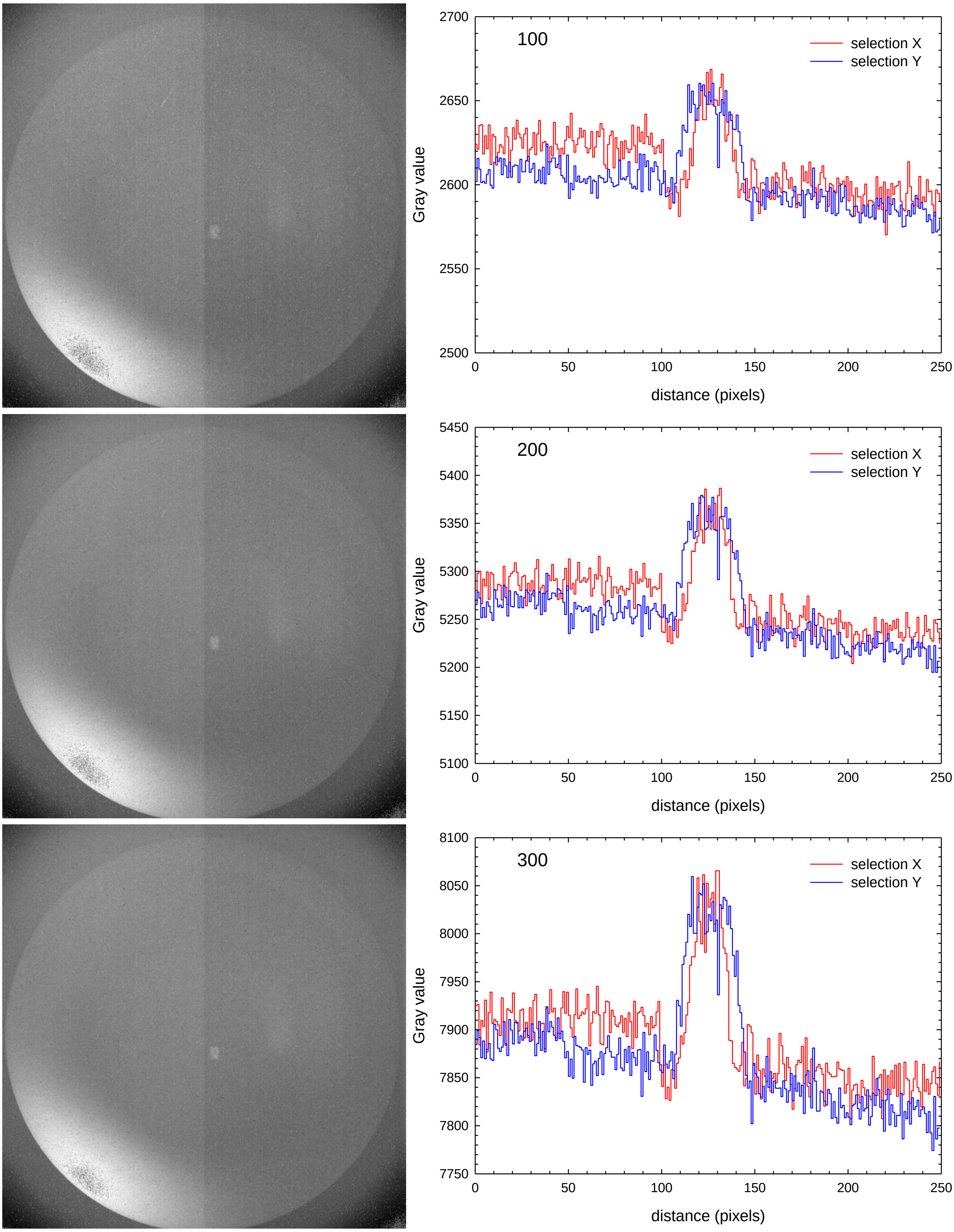

Figure 5.4. Summed images (left); profile on the horizontal (X) and vertical (Y) direction (right).

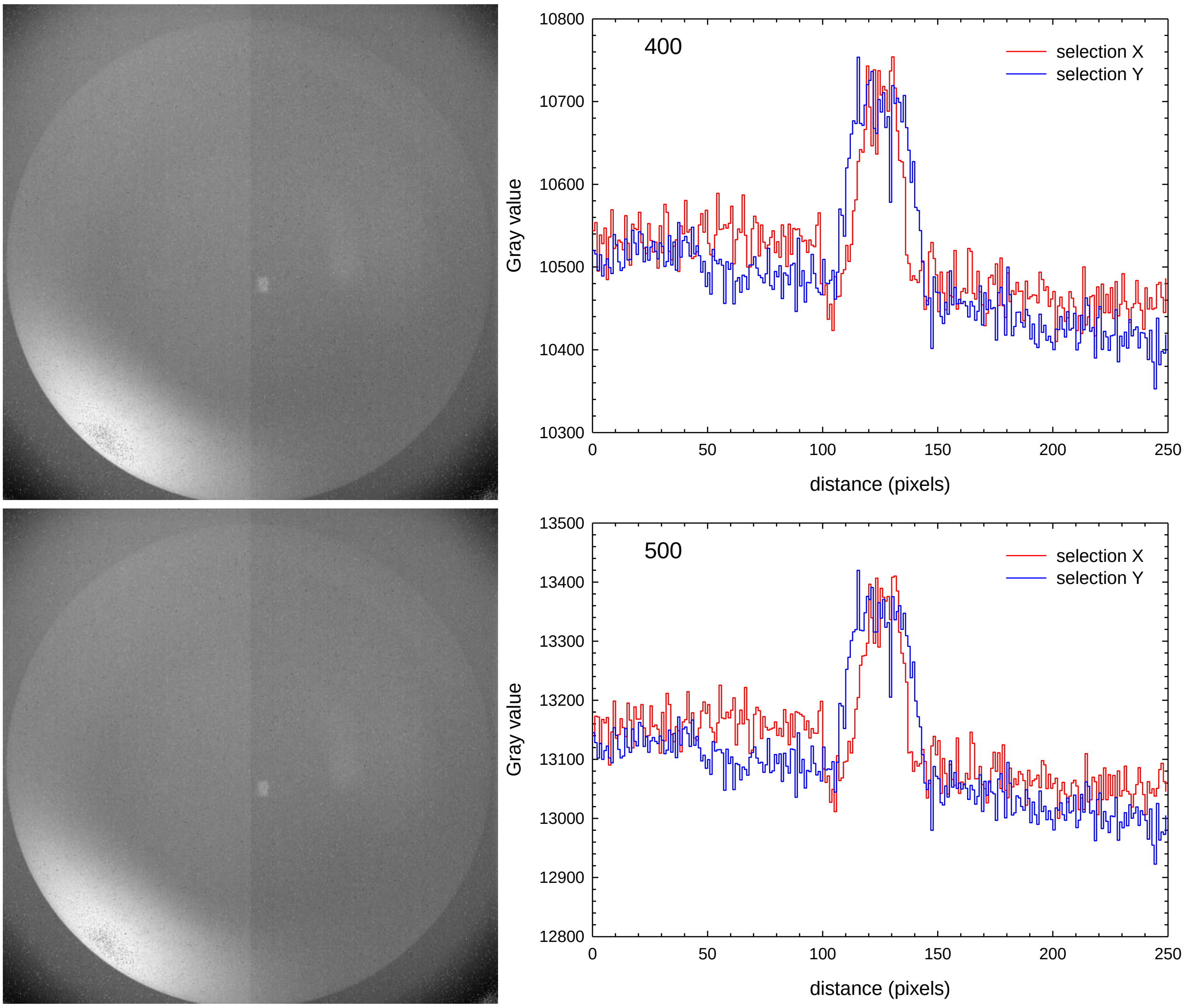

Figure 5.5. Summed images (left); profile on the horizontal (X) and vertical (Y) direction (right).

The profiles in the X and Y directions were obtained after smoothing the signal fluctuations greater than 2 σ. The signal to noise ratio was calculated in the following way:

$$\frac{S}{\sigma_S} = \frac{(S+B)-B}{\sqrt{S+2B}}$$

where B represents the background counts and S the net X-ray signal without the background. For 100 summed images the signal to noise ratio is ~9 and ~21 for 500 added images, improving the contrast in the final image after 1000 s against 200 s. The values are reported in table 5.2:

Table 5.2. Signal to noise ratio values as a function of the acquisition time.

Number of summed images	S/N (Selection X)	S/N (Selection Y)	Acquisition time (s)
100	9.4	9.5	200
200	13.6	13.5	400
300	15.8	16.9	600
400	17.5	19.4	800
500	21.0	21.7	1000

b) Acquisition at high energy

The aim of the measurements was to confirm that the image intensifier is able to record an image generated by a low flux (350 c/s mA cm^2) of high energy photons in not too long an acquisition time, because the detection efficiency at 300 keV is 4% considering that the CsI thickness is 450 μm. Since there was not a source emitting monochromatic gamma rays at 300 keV, the upper limit of the lens bandpass, we have performed some acquisitions by irradiating this detector with a ^{22}Na source, that emits gamma rays at 511 and 1275 keV. In following figure we report the images obtained by illuminating the detector through a Pb collimator (thick = 5 cm, Φ = 1 cm) at different distances from the detector, 0.5 and 9 cm. The acquisition time in the first case is 20 s and we can note that the spot is evident approximately near the detector center, while when the distance increases the spot is less prominent even if we extend the acquisition time up to 100 s.

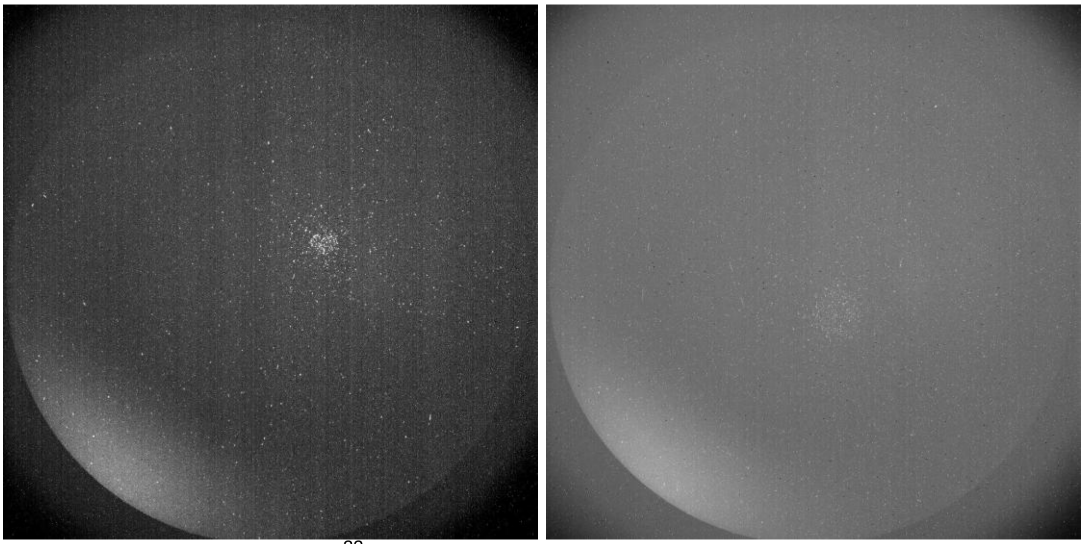

Figure 5.6. Images acquired with ^{22}Na setting a distance detector-collimator of 0.5 (left) and 9 cm (right).

5.2 Detector ALS

The system used comprises an Aluminum Plate with CsI scintillator of 120 mm x 120 mm x 0.5 mm (Hamamatsu), read by a high sensitivity cooled CCD camera system at 12 bit (Apogee) for astronomical and radiological applications, connected to a PC via USB. The detector is a CsI scintillator, grown with a needle like structure resulting in superior resolution, deposited on an Aluminum plate. The ALS detector together with a very smooth mirror mounted at 45°, to reflect the visible light generated by the CsI in the conversion of the incident X rays, is assembled inside a box, that allows electromagnetic shielding and lighting protection. The CCD camera is positioned above the box (see Fig. 5.7), the CCD pixel size is 12x12 microns and the array size is 3056x3056 pixels. After the focusing procedure we have recorded some images (see Fig. 5.8 – 5.11) by irradiating a Laue lens prototype built in the LARIX facility with X rays at 100 keV from an X-ray tube, with a current of 1.2 mA. The lens prototype consists of 20 mosaic crystals made of Copper [111] with a cross section of 15×15 mm2, 3 mm thick and mosaic spread of ~2 to ~3 arcmin. The acquisition time was 60 and 300 s, the binning used was 4 and 5 to enhance the quantum efficiency. The spatial resolution is ~50 μm if the binning is 4 and 60 μm if it is 5, values better than that required.

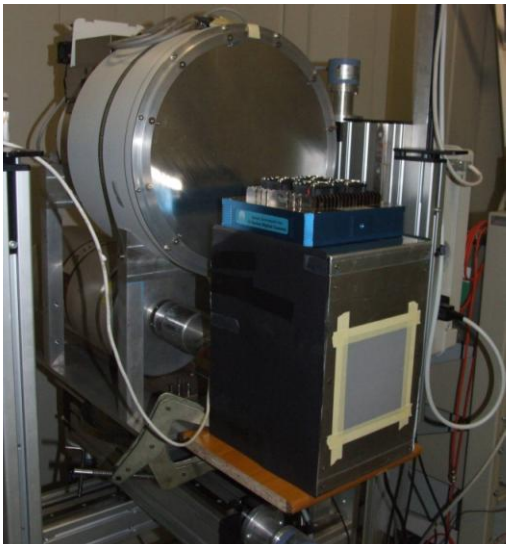

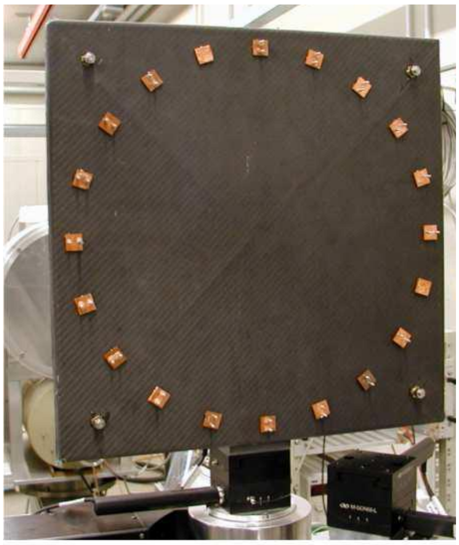

Figure 5.7. (left) the ALS detector at the Larix facility in front of the image intensifier. The blue box on the top is the astronomical CCD camera at 90° with respect to the beam direction; (left) the Lens prototype used for ALS tests.

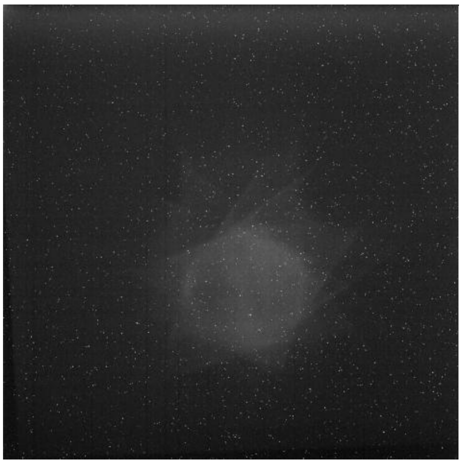

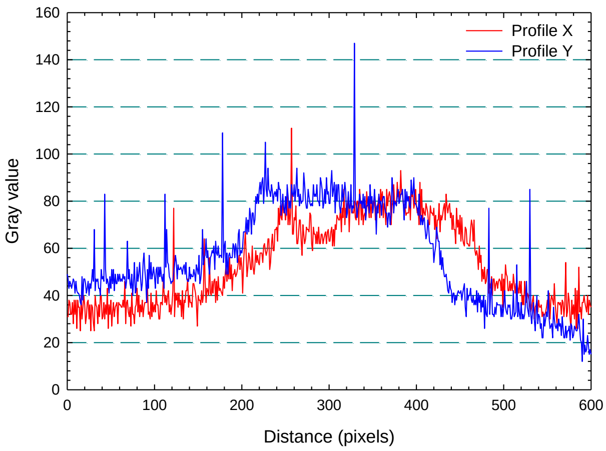

Figure 5.8. Image acquired in 60 s and with binning 4 (left); profile on the horizontal (X) and vertical (Y) direction (right).

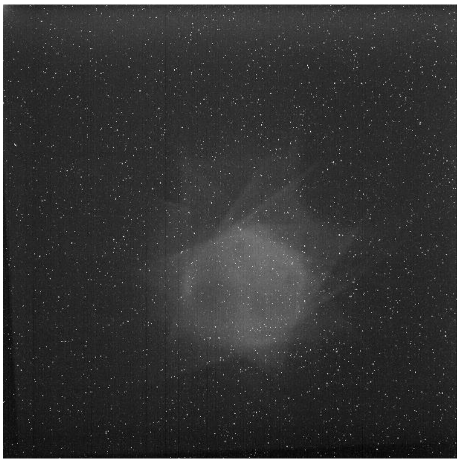

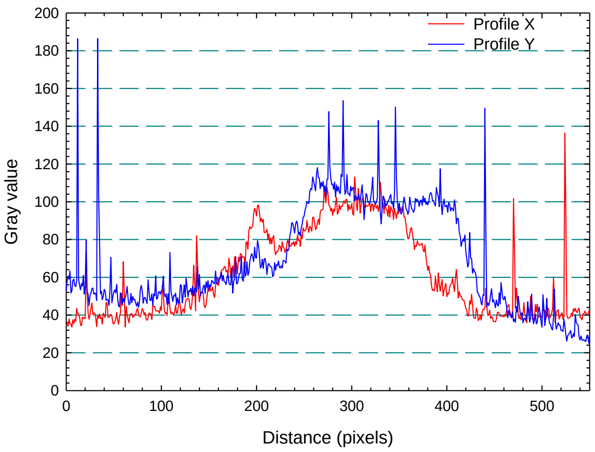

Figure 5.9. Image acquired in 60 s and with binning 5 (left); profile on the horizontal (X) and vertical (Y) direction (right).

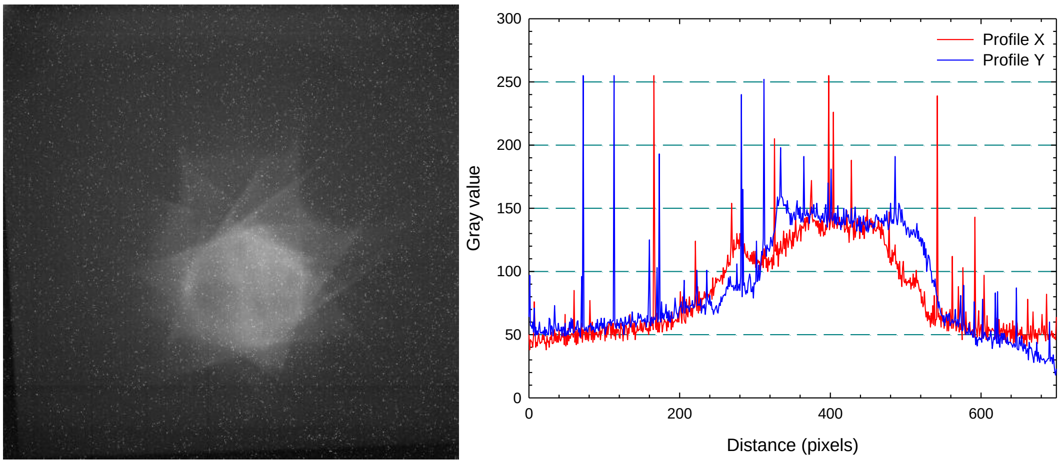

Figure 5.10. Image acquired in 300 s and with binning 4 (left); profile on the horizontal (X) and vertical (Y) direction (right).

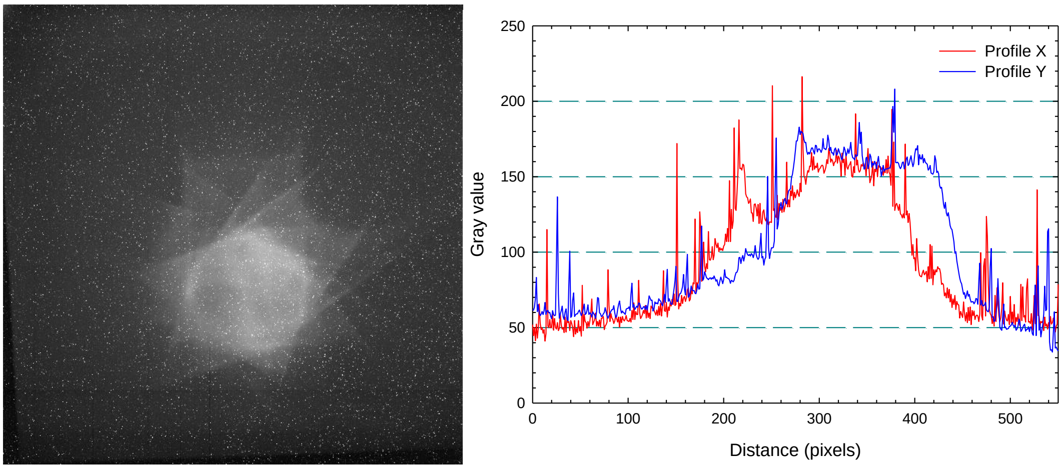

Figure 5.11. Image acquired in 300 s and with binning 5 (left); profile on the horizontal (X) and vertical (Y) direction (right).

It is worth noting that the focal spot is due to the convolution of the spots of each crystal and the relative Signal to Noise ratio increases from 60 to 89 when incrementing the acquisition time from 60 to 300 s. X rays interacting directly with the CCD results in the little white spots in the image, corresponding to the spikes in the X and Y profiles. These spots can be attenuated by careful shielding of the box walls and the CCD with Pb or other high Z materials, furthermore they can be removed by software. The electronics dynamic range is not fully exploited and the S/N ratio is low. In table 5.3 it is reported as a function of the acquisition time and the on chip pixel binning:

Table 5.3. Signal to noise ratio values as a function of the binning and acquisition time.

S/N (Profile X)	S/N (Profile Y)	Pixel binning	Acquisition time (s)
47	61	4	60
60	63	5	60
86	90	4	300
89	91	5	300

In Fig. 5.12 the total and photoelectric efficiency is shown as a function of the energy for several scintillator thicknesses (10% at 300 keV is required).

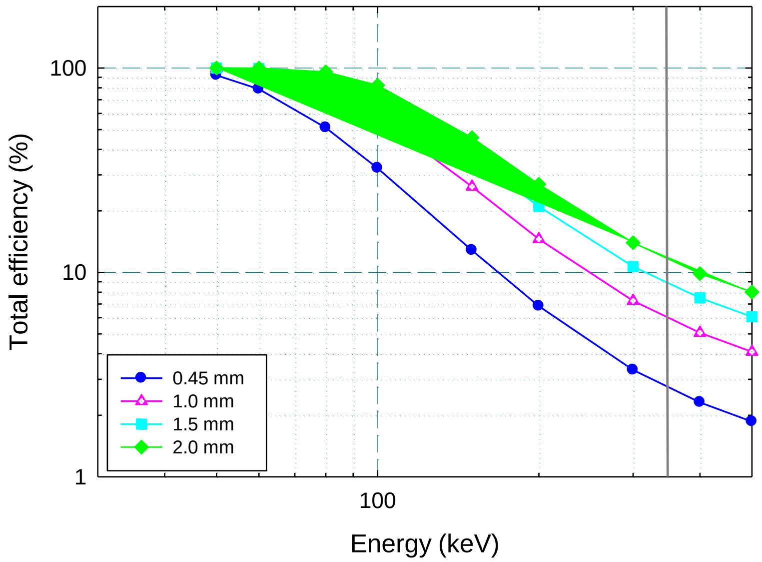

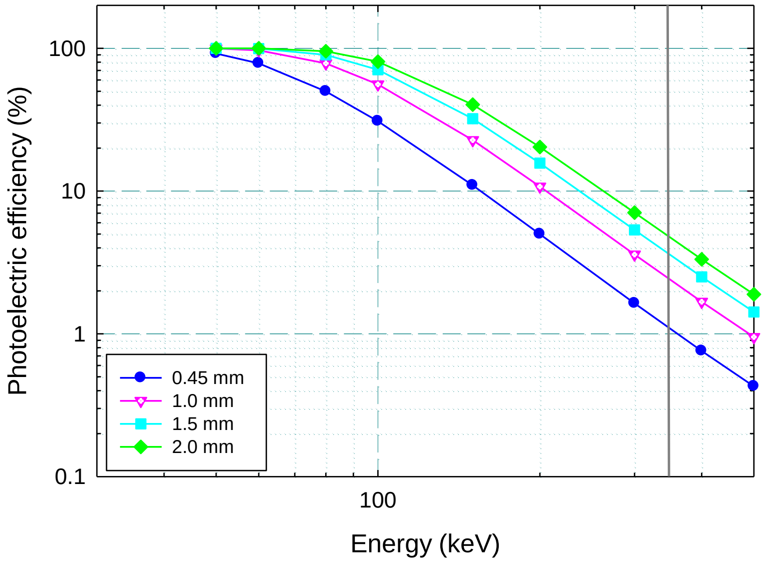

Figure 5.12. Total and photoelectric efficiency of CsI as a function of the energy, calculated at various thicknesses.

5.3 Digital X-ray Flat Panel Detectors

The Digital Flat Panel X-ray Detectors (FPXD) have become available since the 90' s and currently they represent the most current technology for high sensitivity and high resolution imaging in digital radiography both for medical diagnostic and for industrial inspection.
We followed two types of approach to assess the suitablitiy of such a type of imager detector to the Laue Project: (a) measurement with a FPXD device by Hamamatsu provided by colleagues of the Department of Physics at the Bologna University; (b) numerical simulation.

5.3.1 Working principle

The flat panel detector that we have considered exploits the indirect method to convert x rays into an electric charge, as illustrated in Fig. 5.13. In this system the scintillator (CsI or GOS fluorescent screens) is directly deposited on a two-dimensional amorphous silicon photodiode circuitry. When the X rays strike the scintillator, visible light is emitted proportional to the incident X-ray energy. Visible light photons are then converted into an electric charge by the photodiode array, and the charge accumulated in each pixel is converted into a digital value by using the readout electronics, which is sent to a frame grabber.

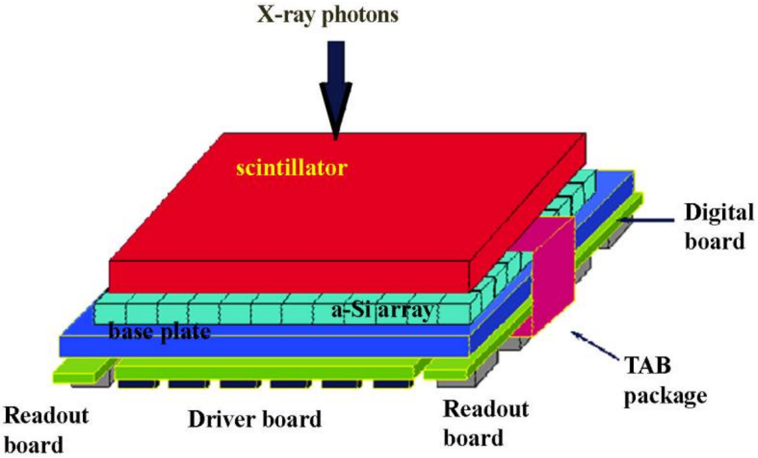

Figure 5.13. Detection principle of a X ray flat panel detector.

5.3.2 Beam Measurments

We have tested a HAMAMATSU digital flat panel of 120 mm x 120 mm and 50x50 µm pixels with a 0.4 thick CsI scintillator at the Larix facility using the same Laue lens prototype decscribed in the previous section. The experimental set up is displayed below.

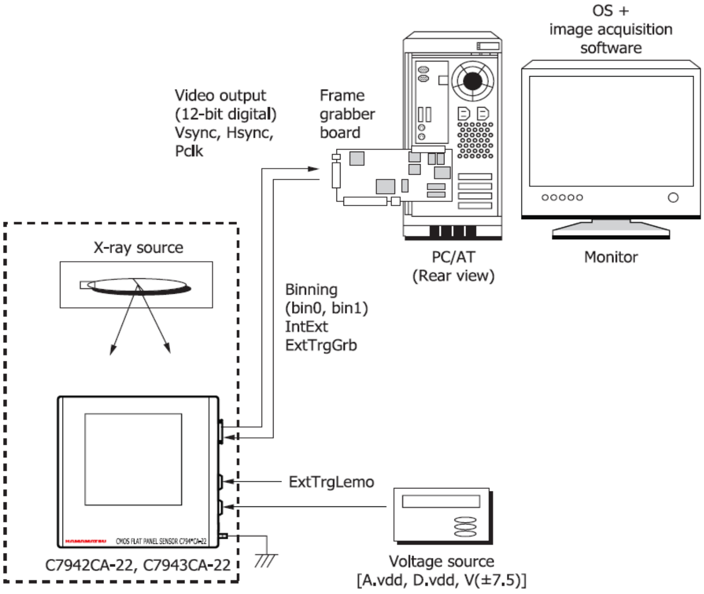

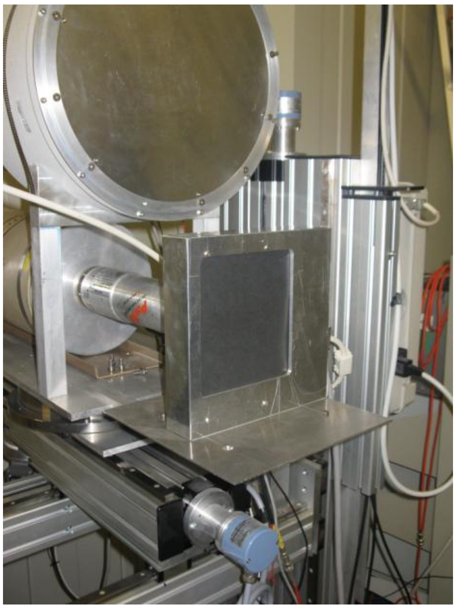

Figure 5.14: (left) Schematic view of the experimental set up comprising the sensor and control board, the exthernal power supply, the frame grabber board; (right) The measurement set up at the LARIX beam facility: the Hamamatsu X ray flat panel detector is positioned below the Thales image intensifier and in front of the HPGe detector.

We acquired images of the background and the transmitted beam at 100 keV (see Fig. 5.15) from a Laue lens prototype, but not of the diffracted beam because the available flat panel and relative software was not optimized for these measurements.
Therefore we have carried out some simulations to verify the response of a digital flat panel detector in the required operating conditions.

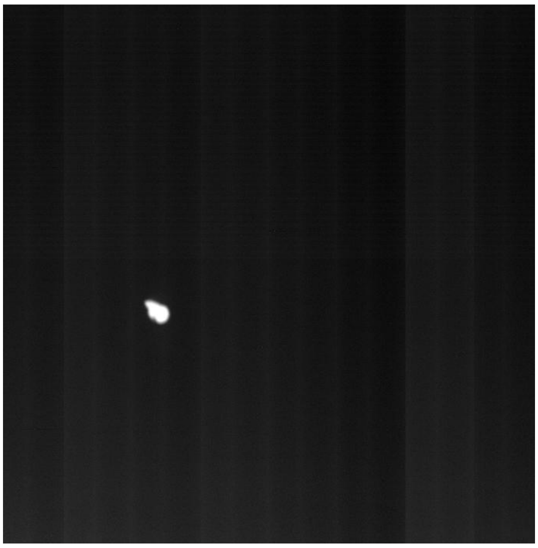

Figure 5.15. The 1s image of the transmitted beam trough the Laue lens obtained by the Hamamatsu FPXD at Larix.

5.3.3 Numerical simulation

In order to evaluate the suitability of FPXD as the focal plane imager for the Laue lens assembling and test, the response of a FPXD has been evaluated by numerical simulation under the expected irradiation conditions at the LARIX Laue beam facility.
As a first step we have evaluated the impinging number of photons over the imager after the Laue diffraction by the crystal tile on the lens support. This evaluation assumed an X-ray tube (350 kVp) as the source. The source is at 20 m from the lens and the lens is at 20 m from the imager. We have supposed that the divergence of the beam after the crystal tile is negligible. Further we have assumed for simplicity that the beam from the crystal tile covers 1 cm^2 (in fact the beam spot will have almost the same surface as the diffracting crystal, i.e. larger than 1 cm^2).

As a second step we have developed an IDL code to evaluate the photoelectric absorption efficiency as well as the scattering efficiency and the energy distribution of scattered photons, assuming a CsI thickness of the FPXD of 0.5 and 1 mm.

Using as input the number of photons impinging on the detector reported in the table of Fig. 5.16,

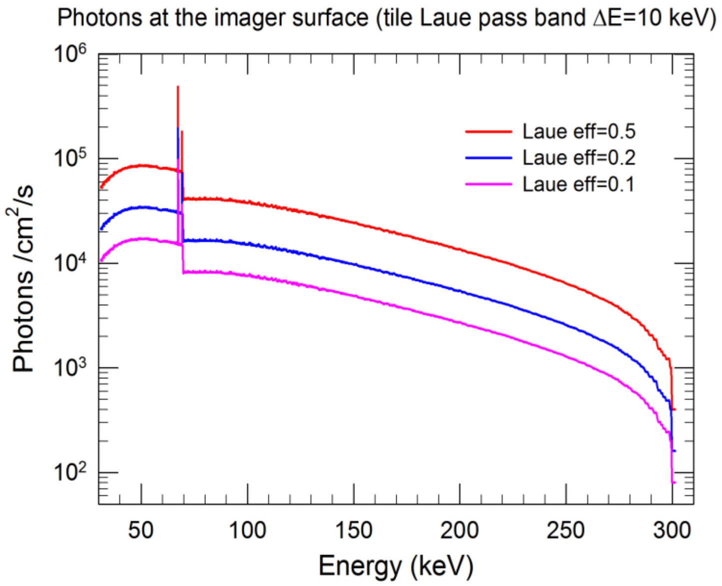

	Crystal diffraction efficiency		
E(keV)	**0.5**	**0.2**	**0.1**
100	37560	15024	7512
150	24523	9809	4905
200	13623	5449	2725
250	6392	2557	1278
300	401	161	80

Figure 5.16: (left) the spectra of diffracted photons impinging on the Focal Imager surface evaluated for 3 different efficiency for crystal diffraction; (top) the table report the number of photons incident in 1 s over 1 cm^2 of the Imager at different energies and integrated over an energy band pass (ΔE) of 10 keV.

we have therefore evaluated the mean energy for each photoelectric interaction (i.e. the impinging energy) and the mean energy of scattered photons.

Table 5.4 reports the number of detected photons (counts) integrated as before in 1 s and over 1 cm^2 divided into counts with full energy deposition (photoelectric events) and in Compton scattered counts. For the latter, the table also gives the average energy released in the CsI scintillator.

Table 5.4. Detected counts and average scattered energy for a 0.5 mm thick CSI FPXD.

Crystal diffraction efficiency = 0.5				*Crystal diffraction efficiency = 0.2*			
Total counts	Photoel. counts	Compton scattered counts	Scattered E mean (keV)	Total counts	Photoel. counts	Compton scattered counts	Scattered E mean (keV)
13249	12642	912	7.5	5299	5057	365	7.5
3467	2972	563	16.0	1387	1189	225	16.0
1030	753	293	26.8	412	301	117	26.8
317	192	130	39.7	127	77	52	39.7
15	7	8	54.2	6	3	3	54.2

These data were then used to evaluate for each count the signal in electrons generated inside the pixel in which the energy was released. In order to perform this transformation we have assumed the parameters reported in table 5.5 to describe both the scintillation process in CsI and the conversion of light into electrons by the Si diodes in the FPXD. The numbers for CsI are from the literature and scintillator provider company data (Saint Gobain/Bicron), while the values used for Si diode readout are derived in a conservative way from values directly discussed with Perkin Elmer (one of the world leader FPXD producers for OEM market) experts.

Table 5.5. Conversion parameters and other information for FPXD response simulation.

CsI scintillation parameters		**Readout Si diode parameters**	
Light photons/keV (*w*)	54	Pixel size	0.2×0.2 mm^2
Max emission wave length	560 nm	Pixels/cm^2	2500
Mean Light photon energy	2.21 eV	Quantum efficiency (Q_ε)	0.5
Light collection efficiency (ε_L)	0.8	Average noise per pixel	4000 e^-

For each count, the energy deposited in the CsI was converted into the current signal using the following relation:

$$N_{e^-} = E_x \cdot w \cdot \varepsilon_L \cdot Q_\varepsilon$$

where Ne^- is the number of electrons generated by each interaction, E_x is the deposited energy, while the meaning of other parameters is defined in the above table.
Finally, the simulation tools generate images integrated over 1 s obtained by distributing uniformly with poissonian statistics the counts/s/cm^2 reported in table 5.4 over a square of 1 cm^2 area (i.e. 2500 pixels). For each count seen by a pixel the signal in electrons is evaluated by the above relation and the result is added to the electrons noise level per pixel per second. The noise is obtained using a random number generator with a poissonian distribution with average of 4000 e^- and σ=sqrt(4000 e^-). The noise is assumed uniformly distributed over all the pixels. Then each 1 s counts image is converted into gray levels assuming 1 gray level every 500 e^- (values given by Perkin Elmer for their FPXD device).

The s/w tools allow the generation of as many 1 second images as the user wants and these images are summed together to achieve the required integration time. The 1 second integration time as been chosen under the indication of Perkin Elmer expert that have suggested integration time up 5 s maximum to avoid pixel saturation. In Fig. 5.17 are reported four images obtained using the simulation tool described above at the two limit operative energies (100 and 300 keV) and integrated over 1 and 100 seconds respectively.

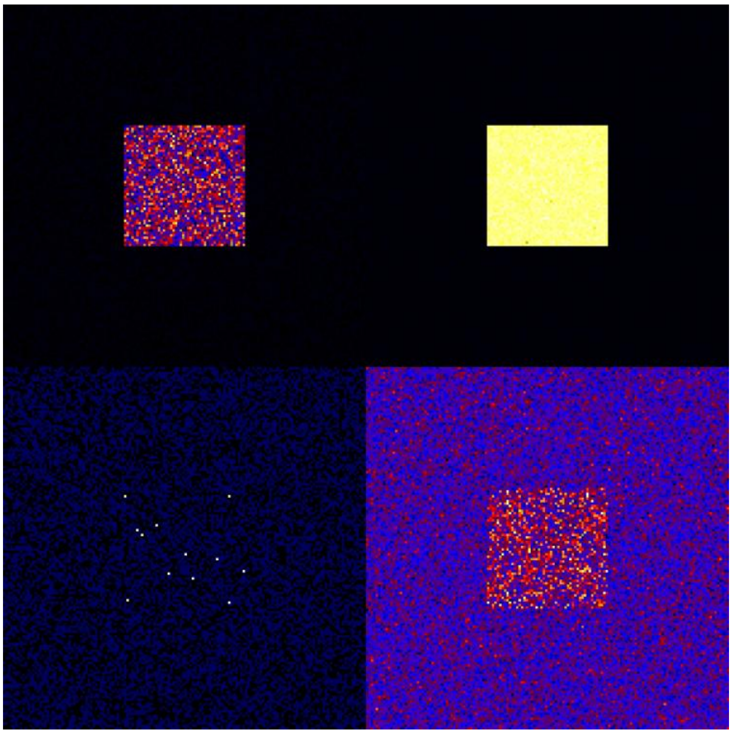

Figure 5.17. FPXD simulated images: (top) in the left 1 s image 100 keV, in the right 100 s image at the same energy; (bottom) in the left 1 s image at 300 keV, in the right 100 s image at the same energy.

The main purpose of the Imager data analysis during the Laue lens assembling is the reconstruction of the position and the tilt of the Laue crystals in order to determine its average diffraction plane and to pass the correct movement parameters to the fine positioner before starting the gluing process for each tile. To determine the Laue diffraction plane average direction with respect the Laue optical axis at a given energy for each crystal we will need to reconstruct both the position of the tile image barycentre and its tilt with respect to the detector axis.

In the simulation we have performed we have limited our analysis to the reconstruction of the tile image barycentre position that is the more critical parameter. In particular, to evaluate the achievable precision, for each integration time our simulation tool calculates the barycentre position of the projected crystal image and evaluates its accuracy (1 σ) in arc-seconds by using the fixed geometry configuration of the lens.

From Fig. 5.18 it is evident that we can achieve the tile barycentre position accuracy within 1 arcsec (as required by the Laue crystal positioning error budget) in less than 100 s for all the energies between 100 and 250 keV. The same plot show that at the higher energy this accuracy limit is not achievable in the same time scale. In fact, extrapolating the data line for 300 keV, we can expect to obtain a 1 arcsec summing at least 500 1s images. In any case the required time is compatible with the requirements of the crystal gluing procedure.

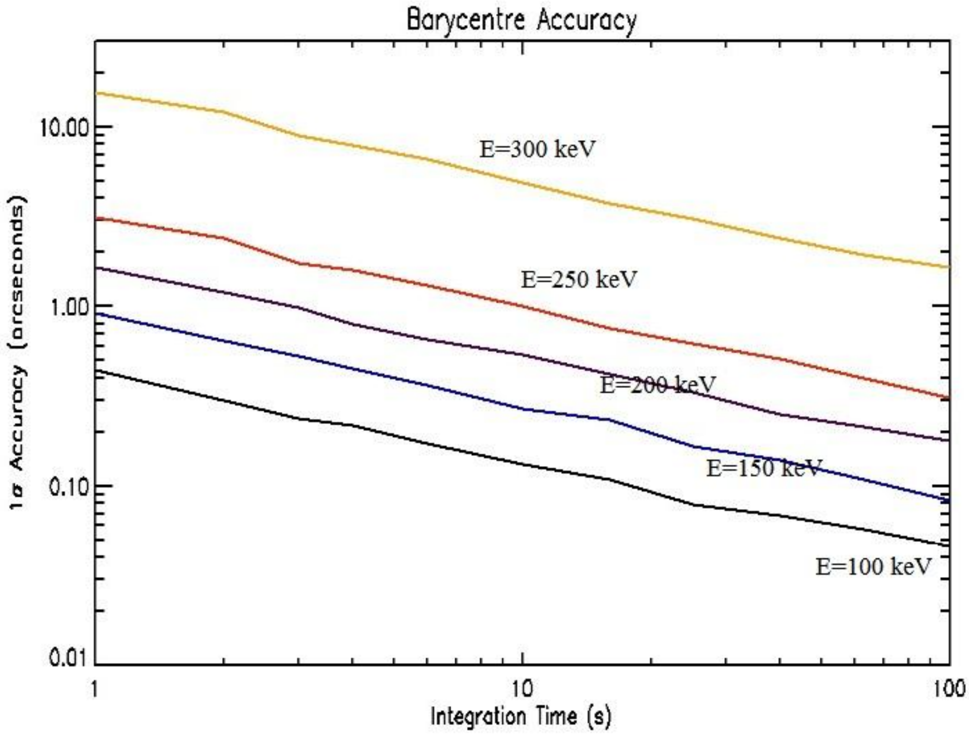

Figure 5.18. The achievable 1 σ accuracy on the crystal spot barycentre obtained from simulated images as function of integration time (i.e. number summed 1s images) for different energies.

6. Spectrometer Requirements

The spectrometers function is to acquire the energy spectrum before and after crystal gluing to verify that it, positioned following the previous procedure, selects the correct energy corresponding to the Bragg angle. The spectrometer chosen to satisfy the requirements described in DA-03 is an High-Purity Germanium (HPGe).

High Purity Germanium has an impurity level of ~1010 impurities per cubic centimeter and is designated either P-type or N-type, based on the type of impurity. One surface of the crystal has a lithium-diffusion N+ layer, ~0.5 mm thick; the other surface has a thinner P+ layer formed by boron ion implantation or gold metallization. When a bias voltage is applied to the crystal, incident ionizing radiation creates charge carriers that are swept toward oppositely charged contacts. In P-type coaxial (IGC series) and well detectors (IGW series), the applied voltage is positive, and holes are the primary charge carriers. In N-type coaxial (NIGC series) and planar crystals (IGP or NIGP detectors), the outer face is the thin P+ layer and the applied bias is negative. Electrons are the main carriers. These detectors have lower trapping levels and are less sensitive to neutron damage.

We have carried out some measurements with radioactive sources using two HPGe detectors, one mounted in the Larix facility and the other available at the Solid State Laboratory of INAF/IASF Bologna. In table 6.1 the detector characteristics are reported:

Table 6.1. Spectrometer specifications.

Detector	**GLP-25300/13 at UNIFE**	**IGP210/1429 at IASF Bo**
Energy range	3 keV - 1 MeV	3 keV - 1 MeV
Detector Sizes (mm^2):		200
active diameter (mm)	25	
sensitive depth (mm)	13	5-20
ΔE(FWHM) at 122 keV (eV)	537 (shaping time 6 μs)	480-610
Peak Shape FWTM/FWHM	1.86	<1.9
Semiconductor material	P-Type HPGe	P-Type HPGe
Detector type and geometry	Planar/LEPS	Semi-Planar
Be Window thickness (mm)	0.25	

6.1 Detector GLP-25300/13

The HPGe detector element, preamplifier and high voltage filter are housed in a detector “capsule” which is attached to an appropriate cryostat or cryostat/dewar. The fully cooled detector system (see Fig. 6.1) is connected to an energy spectroscopic chain, comprising of a Silena spectroscopic amplifier, an external ADC and Multi Channel Analyser.

The spectrum in Fig. 6.2 was acquired with a ^{241}Am source, an amplifier gain of 50 and a shaping time of 2 μs. The bias voltage was -1500 V and the acquisition time 200 s. A zoom of the region at low energy is also shown. The photopeaks were fitted with a Gaussian function, obtaining the following centroids and energy resolutions:

Table 6.2. Centroids and energy resolutions obtained with the detector GLP-25300/13.

Expected centroid (keV)	Measured centroid (keV)	Energy resolution FWHM (eV)
59.54	59.82±0.001	568±2
26.34	26.59±0.02	486±42
20.99	21.13±0.02	779±53
17.80	17.98±0.01	638±16
13.95	14.18±0.01	510±32

Figure 6.1. An example of HPGe detector by Ortec.

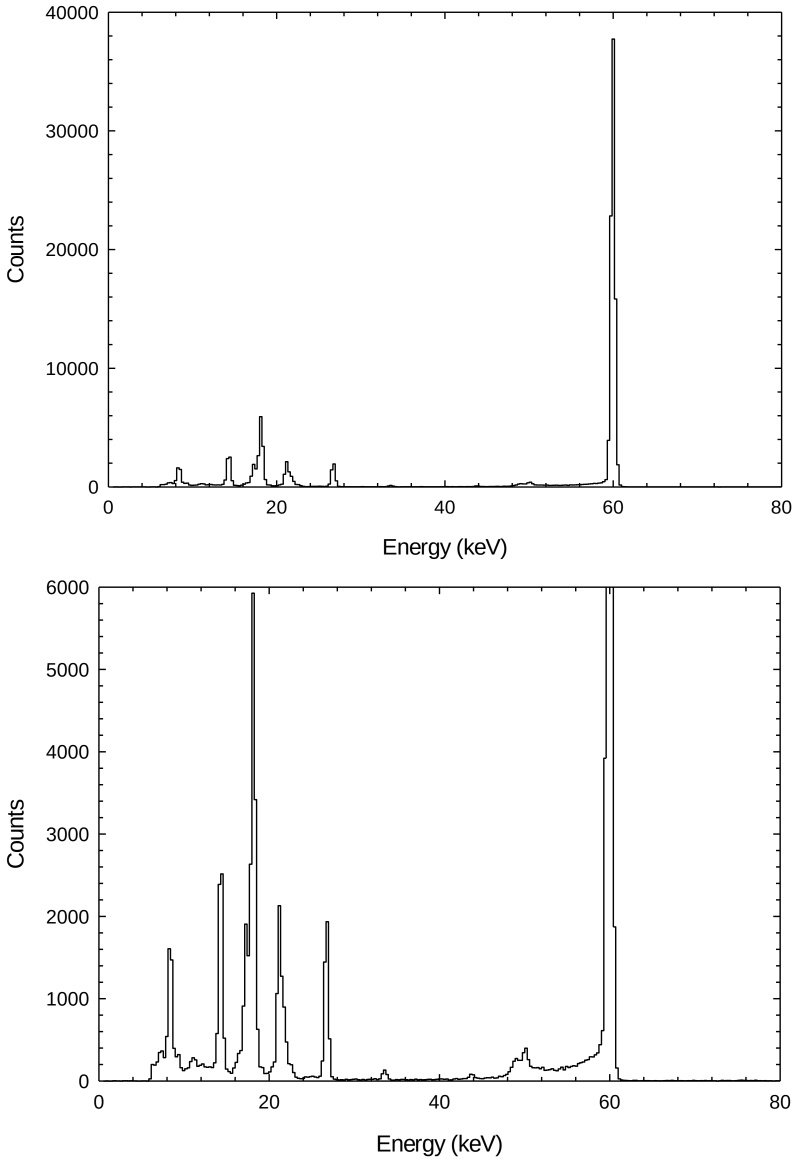

Figure 6.2. ^{241}Am spectrum (top) recorded by irradiating the detector GLP-25300/13; spectrum zoom at lower energies (bottom).

6.2 Detector IGP210/1429

The system used comprises a detecting crystal, FET, preamplifier and an external high-voltage bias supply. The detector and FET are maintained at liquid nitrogen temperature within a cryostat/dewar system. Output is to a multi-channel analyzer (MCA) via a spectroscopy amplifier. The dewar serves as a reservoir of liquid nitrogen (LN2), while the cryostat provides a path via the copper “cold finger” for heat transfer from the detector element to the LN2 reservoir. Both dewar and cryostat rely upon a vacuum to insulate cold inner parts from the room temperature outer surfaces.

The HPGe planar detector is represented schematically in Fig. 6.3.The bias voltage was -2000 V. We have acquired the spectra with a collimated ^{109}Cd source at two shaping time, 6 and 10 μs, of the Ortec amplifiers (Model 450 and 673) as recommended on specification sheet in the range 6-

12 μs. The optimal shaping time is 10 μs at gain 100. In Fig. 6.4 is illustrated the spectrum acquired in 200 s with an inset of the region at 88 keV. The photopeaks were fitted with a Gaussian function, obtaining the centroids and energy resolutions reported in table 6.3.

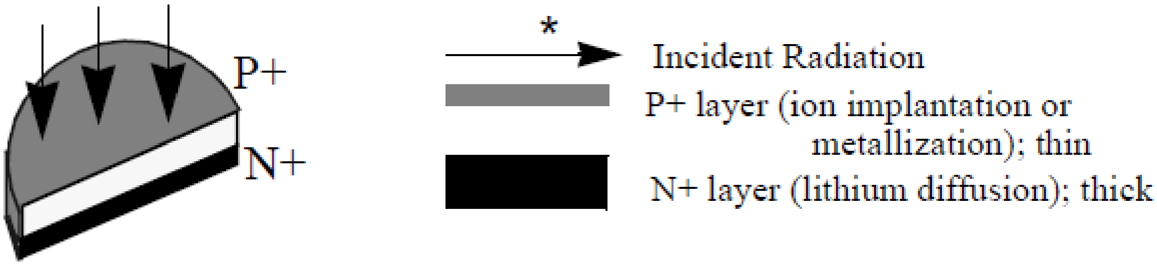

Figure 6.3. Schematic view of the detector IGP.

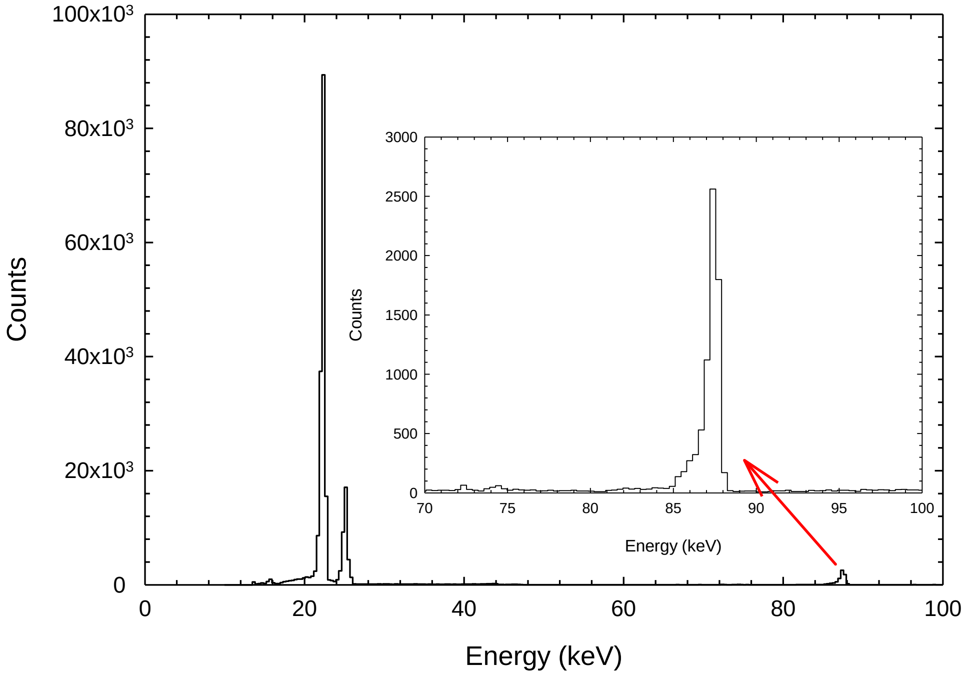

Figure 6.4. ^{109}Cd spectrum recorded by irradiating the detector IGP210/1429.

Table 6.3. Centroids and energy resolutions obtained with the detector IGP210/1429.

Expected centroid (keV)	Measured centroid (keV)	Energy resolution FWHM (eV)
88.04	87.26±0.008	757±18
24.93	24.93±0.02	585±33
22.10	22.15±0.003	510±6

The previous measurements were acquired with a cable that connects the preamplifier and the shaping amplifier both of standard length and long ~ 9 m to simulate the operative functioning at the Larix facility, where the detector and the preamplifier could be mounted in the tunnel while the shaping amplifier and MCA in the control room.

In the following figure the total and photoelectric attenuation is shown as a function of the energy for several detector thicknesses (50% at 300 keV is required).

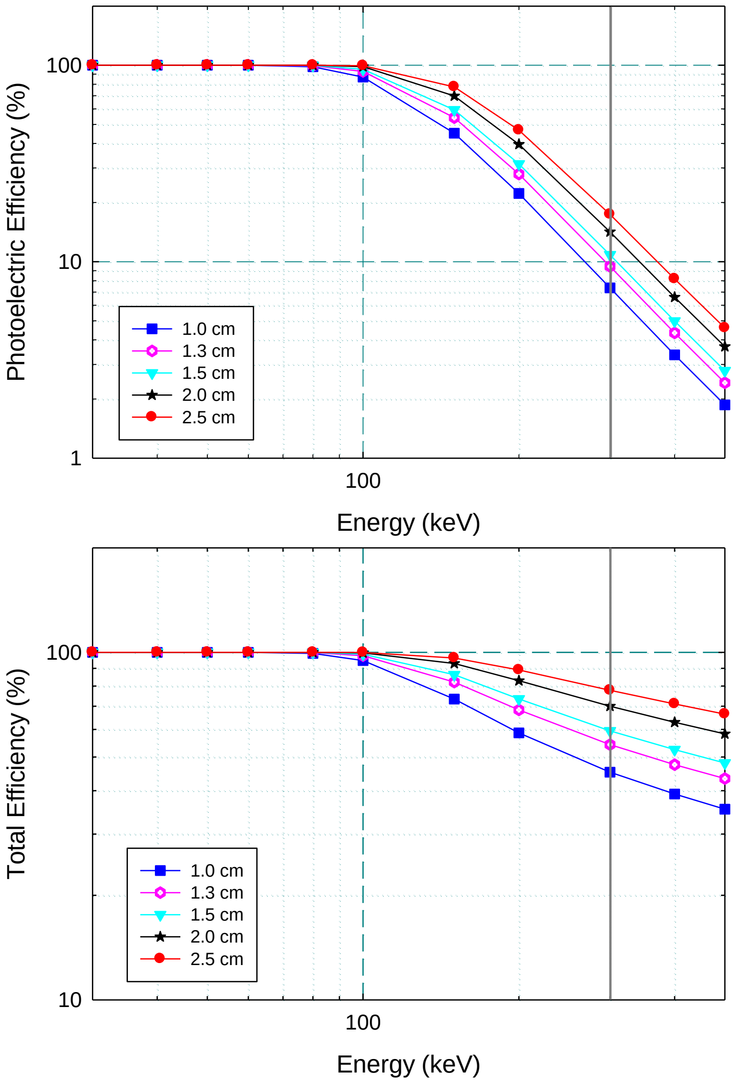

Figure 6.5. Total and photoelectric efficiency of germanium as a function of the energy, calculated at various thicknesses.

Actually we have identified four supplier of the detection system based on High Purity Germanium, ORTEC, CANBERRA, Princeton Gamma Tech and Baltic Scientific Instruments.

7. Identified detector providers and systems

The results of the market research have allowed us to identify three kinds of imaging detectors, image intensifier, ALS detector and digital X-ray flat panel detector.

We have rejected the image intensifier, since it is not readily available because it is obsolete and replaced now by the flat panel detectors. The ALS detector is also not suitable because the electronics dynamic range is not fully exploited.

As Imager, the evaluation we have performed both experimentally and by numerical simulations have allowed us to conclude that the best choice will be a digital flat panel detector. From a market search and analysis we have found that FPXD by PerkinElmer satisfies our requirements because of its high sensitivity, the energy range is 20 keV - 15 MeV, the pixel pitch is 200 μm and the sizes are compatible (29.5 cm x 36 cm x 2.2 cm) and represent a good trade-off between cost and performance with respect to similar products.

We consider the image intensifier as a second choice since this kind of device does not seem readily available because it is based on a technology that is considered almost obsolete in digital radiography for both medical diagnostic and industrial inspection. In fact they are almost completely replaced by X ray flat panel detectors.

The ALS based detector is a solution that can offer a higher sensitivity with the use of very low noise cooled CCD cameras (e.g. astronomical cameras) and finest spatial resolution as well as a larger scintillator thickness range. But to achieve these performance this kind of device require the realisation of a precise and rigid mechanical light tight container for which particular care shall be dedicated in the design of X ray shielding for both the CCD camera and the ALS unit. For these reason this solution have discarded.

Concerning the spectrometer, those actually tested fulfill the requirements (160 eV at 80 keV during the crystal gluing phase; 300 eV at 80 keV during the petal qualification phase).

The detector final suppliers and models are summarized in table 7.1.

Table 7.1. Detector chosen final suppliers and models.

Supplier	Italian representative	Model	Accessories	Procurement time
		Imager		
YXLON	YXLON Semat Equipment S.r.l.	Y.XRS302		
Perkin Elmer		XRD 0822 AO14 XRD 0822 AP14	Power Supply and cables	1-2 months
		Spectrometer		
ORTEC	AMETEK S.r.l. Divisione AMT	GEM-FX5825P4. ORTEC PROFILE FX	Dewar and DSPEC-LF-POSGE	2-3 months
CANBERRA	Tehnology Nuclear Electronics	GL3825R	DSA 1000 and SW	2-3 months
Princeton Gamma Tech		NIGP1010380	System 8008G and SW	2-3 months
Baltic Scientific Instruments	RadTech Strumentazione per Analisi di Fisica Ambientale e Medica	HP(Ge) coaxial detector in Horizontal cryostat	Dewar, MS Hybrid, SW and cables	2-3 months